JAERI-M
6813

NUMERICAL SIMULATION FOR DESIGN OF A TWO-STAGE ACCELERATION SYSTEM IN A HIGH POWER ION SOURCE

November 1976

Yoshihiro OHARA

日本原子力研究所
Japan Atomic Energy Research Institute

この報告書は，日本原子力研究所がJAERI-Mレポートとして，不定期に刊行している研究報告書です．入手，複製などのお問合わせは，日本原子力研究所技術情報部（茨城県那珂郡東海村）あて，お申しこしください．

JAERI-M reports, issued irregularly, describe the results of research works carried out in JAERI. Inquiries about the availability of reports and their reproduction should be addressed to Division of Technical Information, Japan Atomic Energy Research Institute, Tokai-mura, Naka-gun, Ibaraki-ken, Japan.

JAERI-M 6813

Numerical Simulation for Design of a Two-Stage Acceleration System in a High Power Ion Source

Yoshihiro OHARA

Thermonuclear Fusion Laboratory, Tokai, JAERI

(Received November 10, 1976)

In design of the neutral beam injectors for JT-60, the optimum configuration of extraction grids and the operating conditions were studied numerically for a two-stage acceleration in a high power ion source. Results of the calculations show the feasibility to extract a proton beam with energy 75 keV and current 15 A of about 0.6 degree divergence from the 12 cm diameter extraction grids of transparency 40 %. Beam divergence in the two-stage configuration depends largely on the field intensity ratio; the optimum ratio that gives a minimum beam divergence is about 0.3 - 0.5 . Possibility of beam focusing by aperture displacement is also treated with a simple model of thin-lens approximation.

JAERI－M 6813

高出力イオン源の二段加速電極構造設計のための計算機シミュレーション

日本原子力研究所東海研究所核融合研究部
小原　祥裕

（1976年11月10日受理）

ＪＴ－60のための中性粒子入射装置の設計研究の一つとして，二段加速引出し電極構造をもったイオン源の最適構造及び引出し条件を，計算機シミュレーションにより調べた。この結果，透過度が40％で直径が12cmの引出し電極から，エネルギーが75keV，電流が15Ａかつビーム発散が約0.6°のプロトンビームを引出しうることがわかった。又，二段加速電極構造におけるビーム発散は，一段目と二段目の電界強度の比ｆに強く依存し，ｆが0.3～0.5の時，最も小さいビーム発散が得られることがわかった。一方，薄いレンズの近似を用いた簡単なモデルにより，電極孔の"ずれ"によるビーム収束法の可能性についても調べられた。

目　次　な　し

§ 1 Introduction

The neutral beam injection is one of the most powerful and effective methods for heating a tokamak plasma,which has been confirmed in ATC[1], ORMAK[2], CLEO[3],and DITE[4]experiments. The neutral beam with tens of kilovolts energies is now achieved.[5),6),7),8)] However, development of more powerful injectors are desired for the next generation tokamaks such as JET,TFTR and JT-60. Moreover, larger target plasma thickness demands the further increase of beam energy. For these tokamaks, the neutral beam injectors require the ion sources with beam energy of 50-150 KeV, equivarent beam current of tens of ampere and divergence around one degree. However, in the case of single stage acceleration system, the beam power density inevitably decreases with the increase of acceleration energies above some level due to the electrical breackdown problems among extraction grids. This is because the ion current density is space-charge-limited and the breakdown distance for vacuum gaps is practically proportional to the square of an applied voltage.[9)] Namely, the next relations hold,

$$I \propto V^{3/2} d^{-2} \tag{1}$$

$$V_b \propto d^{-1/2} \tag{2}$$

When the gap distance is chosen according to the breakdown distance, we obtain,

$$P_1 = V\, I = C\, V^{-3/2} \tag{3}$$

where C is the constant. Then, the beam power density P_1 may decrease inversely as three-halves power of the acceleration voltage. This restriction is released by decoupling the current extraction stage and the acceleration stage, i.e., by employing a multiple stage acceleration system. If the extraction voltage V is divided into the first stage extraction voltage V_1 and the second stage acceleration voltage V_2 by adding one more grid, then the power density P_2 is given by the relation;

$$P_2 = C\, V_1^{-5/2} (V_1 + V_2) . \tag{4}$$

We find that the power density increases with the increase of the second stage acceleration voltage V_2 , when the total acceleration voltage $V = V_1 + V_2$ is kept constant. Combining the Eq.(3) with Eq.(4), the ratio P_2/P_1 is given by

$$P_2/P_1 = (1 + V_2/V_1)^{5/2} \tag{5}$$

From this relation, we can see that the two stage acceleration system is more advantageous than the single stage system as the ratio V_2/V_1 increases.

There are other advantages in the multi-stage acceleration system.

By adopting the n-stage acceleration system, the breakdown distance becomes n-times smaller than that of the single stage when the total extraction voltage is constant. Therefore, this system reduces the collisions between beam ions and surrounding cold neutrals in the ion acceleration region. In a way it can be said that the breakdown voltage may be $\sqrt{n}$-times larger than that of the single stage if the gap distance is constant.

As for the heat load of the extraction grids, the heat load W scales as follows according to Ref.(10),

$$W \propto n^{-7/4} \qquad (6)$$

Namely, the cooling problems of the extraction grids are reduced with the increase of the stage number n.

The requirements for the ion sources in the JT-60 injectors are as follows;

Ion species : hydrogen
Ion beam current : 15 A
Ion beam acceleration voltage : 75 kV
E-folding gaussian beam divergence : smaller than 1.0°-1.2°
Diameter of the extraction grid : 12 cm
Transparency of the extraction grid : 40 %
Beam duration time : 5-10 sec.

The purpose of this paper is to investigate numerically optimum electrode geometries and operating conditions that satisfy the above requirements.

§ 2. Electrode Geometry of the Two-Stage Acceleration System.

The two stage acceleration system has four electrodes. The first stage is composed of the first and second electrode, and the second stage is composed of the second, third and fourth electrode. Two models (Model A and Model B) have been investigated numerically, as to the two-stage acceleration systems. In the model A, (shown in Fig. 1) the first electrode in contact with a source plasma is multi-aperture type and is held at the positive high potential corresponding to the desired beam energy. The second electrode is also multi-aperture type and spherically concave.

The third electrode is a single disk aperture and is biased at negative potential to suppress the electron backstreaming from the subsequent beam-plasma region. The fourth electrode is also single aperture and is grounded electrically. The optimum configurations in the second stage have already been investigated numerically.[11),12)] In the model B (Fig.1), on the other hand, the first, second, third, and fourth electrodes are all multi-aperture type. In this paper, the optimum configurations in the model B are studied in detail.

There are many parameters in the extraction grids such as aperture diameter, gap distance, grid potential, grid thickness etc.. However, we investigate the effects of four characteristic parameters on the beam optics. They are aspect ratio $a = r_1/d_1$, gap ratio $g = d_1/d_2$, potential ratio $p = V_1/(V_2 + V_3)$, and the field intensity ratio $f = E_1/E_2 = p/g$. Here, r_1 is the radius of the first grid, d_1 and d_2 are the first and the second gap distance, V_1, V_2+V_3, and V_3 are the potential differences in the first, the second and the third gap, and E_1 and E_2 are the electric field in the first and the second gap, respectively. As is shown in Fig.(2), extraction grids form the positive-negative lens when f is smaller than unity and negative-negative lens when f is greater than unity.

§ 3. Computer Simulation Code[13)]

A computer simulation code has been developed for the design of two-stage acceleration system. In this model, the beam emitter surface is determined selfconsistently in such a way that the ion saturation current density is equal to that of the space- charge-limited current. Finite ion and electron temperatures of the source plasma are taken into consideration in the computation of beam trajectories. No ions are emitted from the peripheral region of the emitting surface whose width corresponds to the thickness of the wall sheath λ.[14)] The extracted ions which pass through the zero equipotential surface under the grounded electrode do not suffer from space-charge-expansion because of the presence of electron cloud. Therefore, the beam divergence is defined on the surface.

In order to investigate the validity of this code, computed beam divergences are compared with the experimental data for the same geometry. Experimentally, beamlet characteristics have been measured with the help of the Faraday Cup. Figure (3) shows the comparison of the beam divergence thus obtained. We find that the presence of the wall sheath in the computer code is important for a reasonable agreement with the experiment.

In this paper, the parameters are chosen to be

$$T_e = 10 \text{ eV}, \quad T_i = 1.1 \text{ eV}, \quad \lambda = 0.26 \text{ mm},$$

so that the divergence in the computation agree well with that in experiments. In addition, the edge of the aperture in the first grid is cut as shown in Fig. (3), for the smaller divergence can be obtained by the cutting both in computations and experiments.

§ 4. Results of the Computer Simulations

(1) First, we consider the single stage extraction system composed of multi-aperture over the 12 cm diameter electrode with 40 % transparency. Putting the acceleration gap d is equal to the breakdown distance d_b, we calculate the minimum beamlet divergence and the total extraction current as a function of the aspect ratio. Here, by minimum we mean the optimum beamlet divergence obtained by changing the ion saturation current density of the source plasma. Assuming that all the beamlets have the same divergence, we do not distinguish hereafter the total beam divergence from the beamlet divergence, since we can focus all the beamlets on the focal point without changing the beamlet characteristics.

The breakdown distance d_b in vacuum has been investigated experimentally in some detail by the Culham group.[9] The group presented a relation $V = 60\sqrt{d_b}$ (kV,cm) for the gap distance of 2—5.5 mm, while operating the source. Instead, we take somewhat artificially, the relation $d_b = (V/50)^2$ for the design limit of the gap distance. Since we assume that the potential of the positive and the negative electrodes are 75 kV and -2 kV, respectively, the gap distance is constant and is 2.37 cm. Therefore, Fig. 4 can be regarded as indication of the relation between the beamlet divergence and the radius of the aperture. One may easily understand that it is quite difficult to reduce the beamlet divergence less than 0.75° if we need 75 keV proton beam, and that the beamlet divergence is larger than 1° for the total extraction current of 10 A.

(2) The dominant parameters in the two-stage acceleration system are the aspect ratio, gap ratio, potential ratio and the field intensity ratio as defined in the preceding section. Firstly, the parameter survey has been made by arbitrarily choosing several values of the aspect ratio and the gap ratio. Figure 5(a) shows the dependence of the beamlet minimum divergence ω_{min} on the field intensity ratio f, for the fixed acceleration voltage of 75 kV, where the breakdown limit for the gap distance is neglected. Although it does not cover enough ranges of the parameters,*) one finds that ω_{min} decreases almost proportionally with decreasing f, and does not depend strongly on the aspect ratio and the gap ratio if f is fixed.

We then take into account the breakdown limit for the gap distance using the scaling low of the ion beams. The beam optics is unchanged when the distance scale length is changed. Combination of the equation of motion, Equation of continuity, and Maxwell's equation lead us to the scaling law for the beamlet current and perveance. Namely, if the geometrical length and the applied potential scales as

$$d \rightarrow \alpha d \qquad r \rightarrow \alpha r \quad \text{and} \quad V \rightarrow \beta V$$

then, the beamlet current I and the perveance P scales as

$$I \rightarrow \beta^{3/2}/\alpha^2 I \quad \text{and} \quad P \rightarrow P/\alpha^2$$

For the fixed diameter and transparency of the extraction grids, the number of apertures n scales according to

$$n \rightarrow n/\alpha^2$$

Thus, the total extraction current I_{tot} and the total perveance P_{tot} scales according to

$$I_{tot} \rightarrow \beta^{3/2}/\alpha^4 \; I_{tot}$$
$$P_{tot} \rightarrow P_{tot}/\alpha^4$$

Using the above relations, we scale the gap distance such that either d_1 or d_2 may coincide with the break down limit, while the other still satisfys the relation $d \geq (V/50)^2$. The transparency and the grid diameter are assumed to be the same as in the preceding subsection. Figure 5(b) shows the total current thus obtained. It should again be noted that it does not cover enough ranges of parameters. We only use this figure for the general parameter servey.

---

*) Namely, the gap ratio g is chosen to be less than 1, and the product of a and g is small (less than 0.35).

Above calculations lead us to the following relations, where the notations $\uparrow$, $\downarrow$ and $\sim$ mean the increase, the decrease, and nearly equal respectively.

$$g\ (=\frac{d_1}{d_2})\uparrow \Longrightarrow \begin{cases} d_1\uparrow \Longrightarrow \{\omega_{min}\downarrow \text{ and } P_{opt}\downarrow \\ \text{or} \\ d_2\downarrow \Longrightarrow \{\omega_{min}\downarrow \text{ and } P_{opt}\uparrow \end{cases} \Bigg\} f\ (=\frac{P}{g})\downarrow \Rightarrow \{\omega_{min}\downarrow \text{ and } P_{opt}\downarrow\uparrow$$

$$P\ (=\frac{V_1}{V_2+V_3})\downarrow \Longrightarrow \{\omega_{min}\downarrow \text{ and } P_{opt}\downarrow \Bigg\}$$

$$a\ (=\frac{r_1}{d_1})\downarrow \Longrightarrow \begin{cases} r_1\downarrow \Longrightarrow \{\omega_{min}\sim \text{ and } P_{opt}\downarrow, P_{tot}\uparrow \\ \text{or} \\ d_1\uparrow \Longrightarrow \{\omega_{min}\downarrow \text{ and } P_{opt}\downarrow \end{cases}$$

Here, P_{opt} is the value of P where ω takes the minimum. Thus the appropriate way to decrease ω_{min} and to increase P_{opt} is to decrease d_2. The smaller d_1 gives the larger P_{opt}, but increases ω_{min} simultaneously. Although the smaller r_1 gives the smaller P_{opt}, the total perveance P_{tot} generally increases.

(3) In order to obtain a high extraction current with small beam divergence, both d_1 and d_2 are minimized to the design limit. The design limit here is again chosen to be the breakdown distance $d_B = (V/50)^2$, (cm, kV). Solving a set of equations,

$$\begin{aligned} V_1 &= 50\sqrt{d_1} \\ V_2 + V_3 &= 50\sqrt{d_2} \\ V &= V_1 + V_2 \\ f &= \frac{V_1}{V_2+V_3}\cdot\frac{d_2}{d_1} \end{aligned} \qquad (7)$$

we obtain

$$V_1 = \frac{V + V_3}{1 + f}$$
$$V_2 = \frac{fV - V_3}{1 + f} \tag{8}$$

and

$$d_1 = \left(\frac{1}{50} \cdot \frac{V + V_3}{1 + f} \right)^2$$
$$d_2 = \left(\frac{1}{50} \cdot \frac{f(V + V_3)}{1 + f} \right)^2 = f^2 d_1 \tag{9}$$

Thus, potential differences V_1 and V_2, and distances d_1 and d_2 are uniquely determined in terms of V, f and V_3.

From the designing point of view, there may be a minimum limit on the aperture diameter provided the transparency is kept constant. This is because the grid thickness or the size of the cooling pipe cannot scale too small. In this connection, we fix the aperture diameter around 3.5 mm. Figure 6 shows the dependence of ω_{min} and P_{opt} (I_{tot}) on the field intensity ratio for the proton beam accelerated from the 3.5 mm diam. aperture at V = 75 kV. The extraction electrodes are again 12 cm in diameter and have 40 % transparency. In order to extract total ion current of 15 A,*) f should be larger than 0.6, and the corresponding beamlet divergence ω_{min} is larger than 0.74°. The ion saturation current density J_{sat} required for the source plasma should be greater than 450 mA/cm^2. If f is chosen to be 0.6, and 0.8, potentials and grid distances are summarized in Table 1.

f	V_1 (kV)	V_2 (kV)	d_1 (mm)	d_2 (mm)	ω_{min}
0.6	48.1	26.9	9.3	3.3	0.74°
0.8	42.8	32.2	7.3	4.7	0.80°

Table 1

*) For the ion sources which will be used in the JT-60 neutral beam injectors, we impose 15 A extraction for each 12 cm diam. extractors with overall beam divergence less than 1°- 1.2°.

Figure 7 shows the beam trajectories calculated for typical values of f.

When the gap distances are determined by the equation $d = (V/40)^2$ instead of $d = (V/50)^2$, a larger safety factor is included against breakdowns but less currents are extracted from the same diam. grids (See Fig. 8). In this case, the beamlet divergence becomes greater than 1.2°, if one tries to extract 15 A. Thus the critical gap distance as imposed on the grid design basis influences the beam property significantly. In this connection, a problem remains about to what ranges or in what conditions the Culham's empirical law can be extrapolated in the case of multi-stage extraction system. For instance, the critical distance may presumably be influenced by the presence of working gas introduced into the grid region, or by the presence of impinging ions and/or secondary electrons on and from the aperture edges.

(4) To improve the beam divergence, two approaches are considered. The one is to change the radius of the aperture, and the other is to increase the gap distance. In the preceding subsection, the grid distances are chosen to be equal to the breakdown limit. Here, we increase either d_1 or d_2 greater than the design limit.

Firstly, the aperture diameter is changed with other parameters remain unchanged. The results are shown in Figs.9(a),9(b) and 9(c), where the aperture diameter is chosen to be 2.8 mm, 4.0 mm and 4.5 mm, respectively. It is found that the minimum value of the beam divergence is not improved in any case. However, the beamlet divergence at the extraction of 15 A decreases with decreasing aperture diameter, although it saturates to decrease for the aperture radius less than 3.5 mm. The results are summalized in Fig.10.

Secondly, the gap distance is increased such that either d_1 or d_2 becomes greater than design limit. The parameter f decreases with increasing d_1, and increases with increasing d_2. The results are shown in Fig. 11, where the beam divergence and the total current change appreciably when the gap distance is increased from the reference point denoted by the circles at f = 0.5, 0.8 and 1.2 (where the gap distances are minimized to the design limit). In consequence, the beam divergence is not improved and moreover, the extraction current decreases significantly.

Thus it may be recommended that the aperture diameter should be 3.0 - 3.5 mm and the gap distances be equal to the breakdown design limit.

(5) In Fig.5, the minimum beam divergence decreases with decreasing field intensity ratio and is less than 0.5 degree for $f \leq 0.5$, although the extraction current is low. In Figs.6-10, however, the minimum beam divergences saturate to decrease with decreasing f. Here, we will investigate this discrepancy and try to improve the beam divergence without losing high extraction current. We find that the 2nd aspect ratio a_2, defined by the radius of the second stage acceleration aperture r_2 divided by the second gap d_2, is the important parameter. Namely, in Fig.5, $a_2(=a \cdot g)$ is always less than 0.35, while in Figs.6-10, a_2 is much larger for small values of f.*) Indeed, the decrease of f is effective in reducing the beam divergence, provided the field intensity ratio represents the approximate value on the aperture axis. When a_2 is large, however, the electric field is strongly deformed near the aperture axis as shown in the latter half of Fig.7. Thus, even if f is less than 0.5, the value of f_{axis} (the field intensity ratio defined at the aperture axis) is much larger, and therefore the minimum beam divergences are not improved. To overcome this difficulty, two methods may be considered. The first one is to decrease the 2nd aspect ratio a_2 without changing other parameters. In order to achieve this situation, the aperture diameter of the 2nd positive and negative grids are decreased. The second way is to apply three-stage acceleration system by adding one more grid (the third positive grid) and to make thus combined 2nd and the 3rd electric field approach uniform.

For the first way, we find that the minimum beam divergence can be reduced by 0.05° when $2r_2$ and $2r_3$ are decreased from 3.5 mm to 2.45 mm (a_2:1.39 → 0.97) for the case of f = 0.3. For the second way, the potential difference between grids V_i and the gap distance d_i are given by

$$V_1 = \frac{V + V_4}{1 + f_1 + f_1 f_2}$$

$$V_2 = \frac{f_1(V + V_4)}{1 + f_1 + f_1 f_2} \qquad (10)$$

$$V_3 = \frac{f_1 f_2 V - (1 + f_1)V_4}{1 + f_1 + f_1 f_2}$$

*) For instance, a_2 = 0.70, 0.95 and 1.46 corresponding to the latter three cases in Fig.7 .

and

$$\begin{aligned} d_1 &= (V_1/50)^2 \qquad (\mathrm{kV,cm}) \\ d_2 &= (V_2/50)^2 = f_1^2 d_1 \\ d_3 &= (V_3+V_4/50)^2 = f_1^2 f_2^2 d_1 \end{aligned} \tag{11}$$

where f_1 and f_2 are defined by

$$\begin{aligned} f_1 &= \frac{E_1}{E_2} = \frac{V_1 d_2}{V_2 d_1} \\ f_2 &= \frac{E_2}{E_3} = \frac{V_2 d_3}{(V_3+V_4) d_2} \end{aligned} \tag{12}$$

We calculate next two cases assuming the aperture diameters

$$2r_1 = 2r_5 = 3.5 \text{ mm} , \quad 2r_2 = 2r_3 = 2r_4 = 2.45 \text{ mm} .$$

(a) $f_1 = f_2 = 0.5$

(b) $f_1 = 0.37, \quad f_2 = 1.0$

Figure 12 shows the beam trajectories for the above cases. We find that the minimum beam divergence is reduced to 0.58° and 0.63° in the case (a) and (b), respectively. Thus the beam divergence is improved by 0.1° by introducing the three stage acceleration system.

§ 5. Beam Focusing by Aperture Displacement in the Two-Stage Acceleration

In order to increase the injection power through the limited area of the ports, it is necessary to focus the beamlets from the multiaperture electrodes at a point of several meters apart from the source. There are two methods in focusing the beamlets; one is by aperture displacement,[15] and the other is by curved electrodes. In the latter case, extraction grids should be concave so that the curvature center of the grid is the focal point. For instance, the 12 cm diam. grid shall be curved only by 0.36 mm compared with plain disk grid at the axis, if we need the focal point 5 m apart from the grid. Assuming the machining inaccuracy of $\pm$ 0.1 mm, the focal point ranges between 3.6 and 6.4 m.

On the other hand, the focusing by aperture displacement is investigated both in experiments and in a simple model in thin lens approximation. Now, we intend to apply this simple model to the focusing of two-stage acceleration. An aperture with a different potential gradient on each side acts as a lens with focal length $F=4V/(E_2-E_1)$ where E_1 and E_2 are, respectively, the electric field on each side of the extraction grid, and eV is the energy of the beam which pass through the grid. Two-stage acceleration system consists of two lenses. The first lens is formed by the electric field in the first and the second gap, and the second lens is formed by the electric field in the second and the third gap. The electric field in the third gap, however, is almost negligible compared with the others. According to the results of the computer simulation, $E_1 = k_1 V_1/d_1$ with $k_1 = 0.9 \sim 1.0$ and $E_2 = k_2(V_2+V_3)/d_2$ with $k_2 = \sim 1.0$ in the wide range of the beam current density, if the gap distances are enough larger than the aperture radius. Therefore, we choose $E_1 \doteq V_1/d_1$ and $E_2 = (V_2+V_3)/d_2$, though in the single stage acceleration the deflection angle by aperture displacement agrees well with the experimental results when we put $E_1 = 4V_1/3d_1$ in the plane parallel approximation.[15] The focal length of the first and the second lenses are given as follows;

$$F_1 = 4V_1/(E_2-E_1) = 4d_2pg/(g-p)$$
$$F_2 = 4(V_1+V_2)/(E_3-E_2) = -4d_2(1+p) \qquad (13)$$

There are three cases in the aperture displacement of the two-stage configuration, which are the displacement of the first grid(a), the second grid(b) and the third grid(c), respectively(Fig.13). The ratios of reflection angle of the beamlet θ to the displacement of the grid Δ are given as follows for each case,

$$\text{(a)}\ \frac{\theta}{\Delta_1} = \left(\frac{1}{F_2} - \frac{1}{d_2-F_1}\right)\frac{F_1-d_2}{F_1} = \frac{5g-5p-4p^2}{16d_2p(1+p)g}$$
$$\text{(b)}\ \frac{\theta}{\Delta_2} = \left(\frac{1}{F_2} - \frac{1}{d_2}\right)\frac{d_2}{F_1} = \frac{(4p+5)(g-p)}{16d_2p(1+p)g} \qquad (14)$$
$$\text{(c)}\ \frac{\theta}{\Delta_3} = \frac{1}{F_2} = -\frac{1}{4d_2(1+p)}$$

The first two cases are inadequate for the displacement characteristic depends largely on the parameters d_2, p and g. In the third case, however, the deflection depends only d_2 and p (Fig.14), and the dependence is more weak than the others. The displacement must satisfy the following inequality in practice;

Machining Inaccuracy $\pm$ 0.1 mm << Δ << Aperture Diameter $\sim$ 3.5 mm. Now, when p=0.5, d_2=8 mm, focal length F=4.5 m, and the diameter of extraction grid of 12 cm, the displacement Δ_3 is equal to about 0.5 mm. This is the practical value of the displacement. Consequently, the beam focusing by aperture displacement is also possible for the case of two-stage configuration.

§ 6. Conclusion

As one of the design works of the neutral beam injectors for JT-60, the optimum configurations of the extraction grids and operating conditions have been examined numerically in the two-stage acceleration system. The possibility of beam focusing by aperture displacement is also investigated by applying a simple model in the thin lens approximation.

From our computational results, we find it possible to obtain a proton beam with energy of 75 KeV, current of 15 A and divergence of about 0.6 degree from the 12 cm diam. extraction grids with 40 % transparency. In this computation, the effects of the ion and electron temperature of the source plasma on the beam optics are included. But, there are other factors which increase the total beam divergence. In the first place, the total beam is obtained through the extraction grids with hundreds of apertures, while the computation is carried out on the beamlet. Therefore, the aberration may be increased not only by mechanical error of the grids' system but by deformation of the grids by heat loads. Due to these errors, some of the beamlets are also deflected and the injection power through the port may be reduced. Namely, the divergence increases effectively. In the second place, the divergence may be increased by the fluctuation and density gradient over the extraction grid in the source plasma. In the third place, although the actual beam

is composed of atomic and molecular ions, the effects of mixed species on beam charecteristics are not considered in the computation. Finally, the collisions such as charge exchange, ionization and desociation are not considered in the ion acceleration region. In addition, the ions are not extracted from the subsequent beam plasma region. These effects may change the beam optics as well as increase the heat load of the grids. Consequently, the divergence of the actual multiampere beam becomes larger than that of computation by about zero point several degree.

The electrical breakdown among extraction grids has important effects on the beam characteristics. It is necessary to investigate the breakdown condition above tens of kilovolts, which may depend, for example, on the gas pressure between the grids and the materials of the grids.

It is found that the beam divergence in the two-stage configuration depends strongly on the field intensity ratio f, and the optimum value of f that gives the minimum beam divergence is about 0.3 - 0.5 . It also depends on the second stage aspect ratio a_2, which in turn affects the field intensity ratio on the beamlet axis. The three-stage acceleration is superior to the two stage in that the smaller field intensity ratio is easily obtained on the axis of the aperture when the gap distance is chosen according to the breakdown distance.

On the other hand, we see that the beam focusing by aperture displacement is also available in the two-stage acceleration system, where the displacement of the third grid is more adequate than that of the first or the second grid.

Acknowledgements

The author acknowledges the valuable discussions with and suggestions from S. Matsuda. Thanks are also due to H. Shirakata and S. Mori for their support and encouragement.

References

1) K. Bol et al.;Phys. Rev. Letters, 32(1974), 661.
2) L. A. Berry et al.; Plasma Physics and Controlled Nuclear Fusion Research (Proc. 5-th Intern. Conf. Tokyo, 1974)IAEA-CN-33/A5-2.
3) J. G. Cordey, et al.; CLM-P383, Feb. (1974).
4) J. W. M. Paul, K. B. Axon et al.; Plasma Physics and Controlled Nuclear Fusion Reseach (Proc. 6-th Intern. Conf. Berchtesgaden, 1976)IAEA-CN-35/A17.
5) R.C.Davis, et al.; ORNL-TM-4657, Aug. (1974).
6) W. R. Baker et al.; LBL-3208, Sep. (1974).
7) D. A. Aldcroft et al.; CLM-P414, Feb. (1975).
8) M. Fumelli ; EUR-CEA-FC-809, Feb. (1976).
9) J. R. Coupland et al.; Rev. sci. Instrum. 44, 1258 (1973).
10) L. D. Stewart et al.; 1-st Topical Meeting on the Tech. of Controlled Nuclear Fusion, San Diego, (1974).
11) T. Sugawara and Y. Ohara ; Japan. J. appl. Phys. 14, (1975)1029.
12) Y. Ohara and T. Sugawara ; JAERI-M 5929 (1974)
13) Y. Ohara ; JAERI-M 6757 (1976), in Japanese.
14) S. A. Self ; Phys. of Fluids, 6, 1762 (1963).
15) L. D. Stewart, J. Kim and S. Matsuda ; ORNL-TM-4920, May (1975).

Figure Captions

Fig. 1. Two models of the two-stage acceleration system (Model A and Model B).

Fig. 2. Illustration of lens actions in the two-stage acceleration system.

Fig. 3. Comparison of the measured beam divergence with calculated one.

Fig. 4. Dependence of the minimum beamlet divergence of the 75 KeV proton beam on the aspect ratio a in the case of single stage acceleration. The accel gap distance is fixed to be 23.7 mm.

Fig. 5. Dependence of the minimum divergence on the field intensity ratio f for the fixed acceleration voltage of 75 kV (a), and the dependence of the total extracted current from the 12 cm diam. grids with 40 % transparency on f , where the gap distances are scaled such that either d_1 or d_2 may coincide with the breakdown limit, while the other still satisfys the relation $d > (V/50)^2$.

Fig. 6. Dependence of ω_{min} and P_{opt} (or I_{tot}) on the field intensity ratio for the proton beam accelerated at V=75 kV from the 3.5 mm diam. aperture, where gap distance d_1 and d_2 are chosen to be the breakdown limit.

Fig. 7. Beam trajectories calculated by the computer code IONORB for typical values of f ; (a) f=1.2, J=600 mA/cm^2, ω=1.04 , (b) f=0.8, J=500 mA/cm^2, ω=0.83 , (c) f=0.5, J=400 mA/cm^2, ω=0.77 ,(d) f=0.4, J=350 mA/cm^2, ω=0.72 , (e) f=0.3, J=300 mA/cm^2, ω=0.74 .

Fig. 8. Dependences of ω_{min} and P_{opt} (or I_{tot}) on f, when the gap distances are determined by the equation $d = (V/40)^2$ (kV,cm) instead of $d = (V/50)^2$.

Fig. 9. Dependence of ω_{min} and P_{opt} (or I_{tot}) on f, where the aperture radius is chosen to be 2.8 mm (a), 4.0 mm (b) and 4.5 mm (c).

Fig.10. Relation between the divergence and the aperture diameter, where the total current is fixed to be 15A.

Fig.11. Changes of the beamlet divergence and the total extraction current (triangular points), when the gap distance is increased from the reference points denoted by the circular points at f=0.5, 0.8 and 1.2 .

Fig.12. Typical examples of beam trajectories in the three-stage acceleration system ; (a) f_1=0.5, f_2=0.5, J=550 mA/cm^2, ω=0.58 and (b) f_1=0.37, f_2=1.0, J=400 mA/cm^2, ω=0.63 .

Fig.13. Three cases of beam focusing by aperture displacement in the two-stage configuration. Displacement of first extraction grid (a), second grid (b) and third grid (c).

Fig.14. Ratio of deflection angle to the displacement distance versus potential ratio p, when the third grid is displaced.

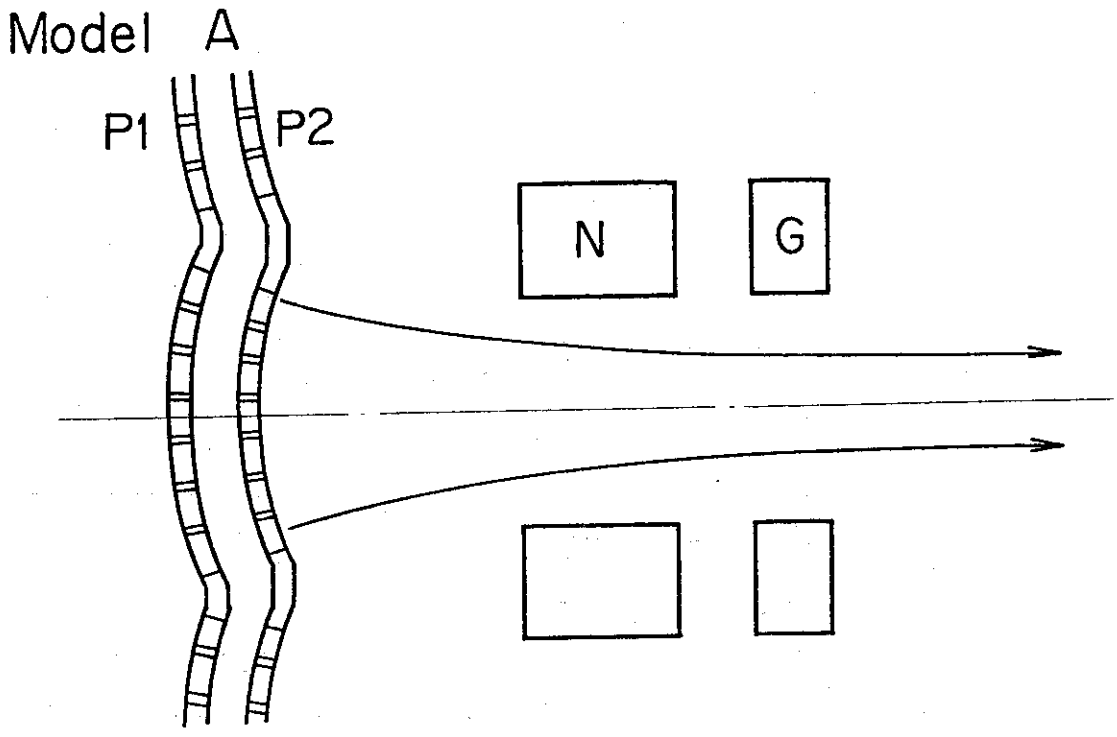
Model A
P1
P2
N
G

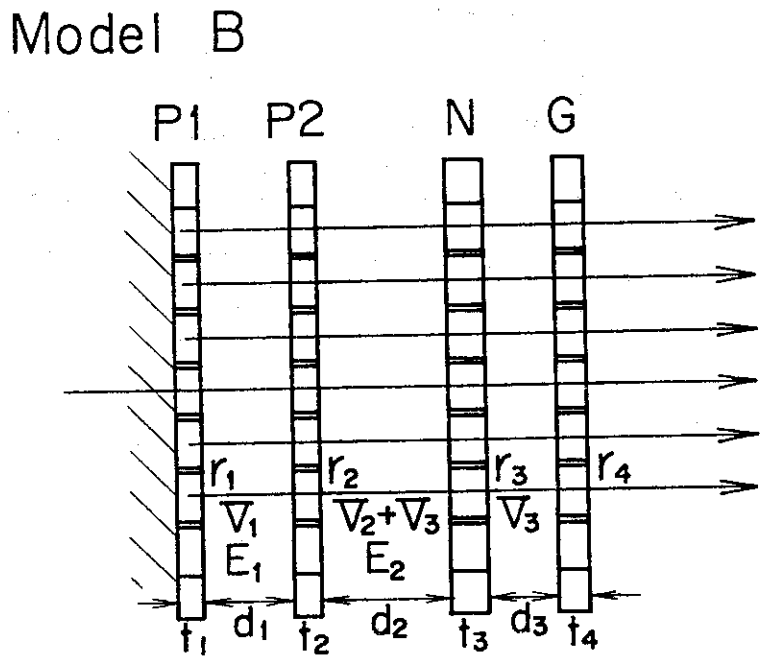
Model B
P1
P2
N
G
r1
r2
r3
r4
V1
V2+V3
V3
E1
E2
d1
d2
d3
t1
t2
t3
t4

Fig. 1

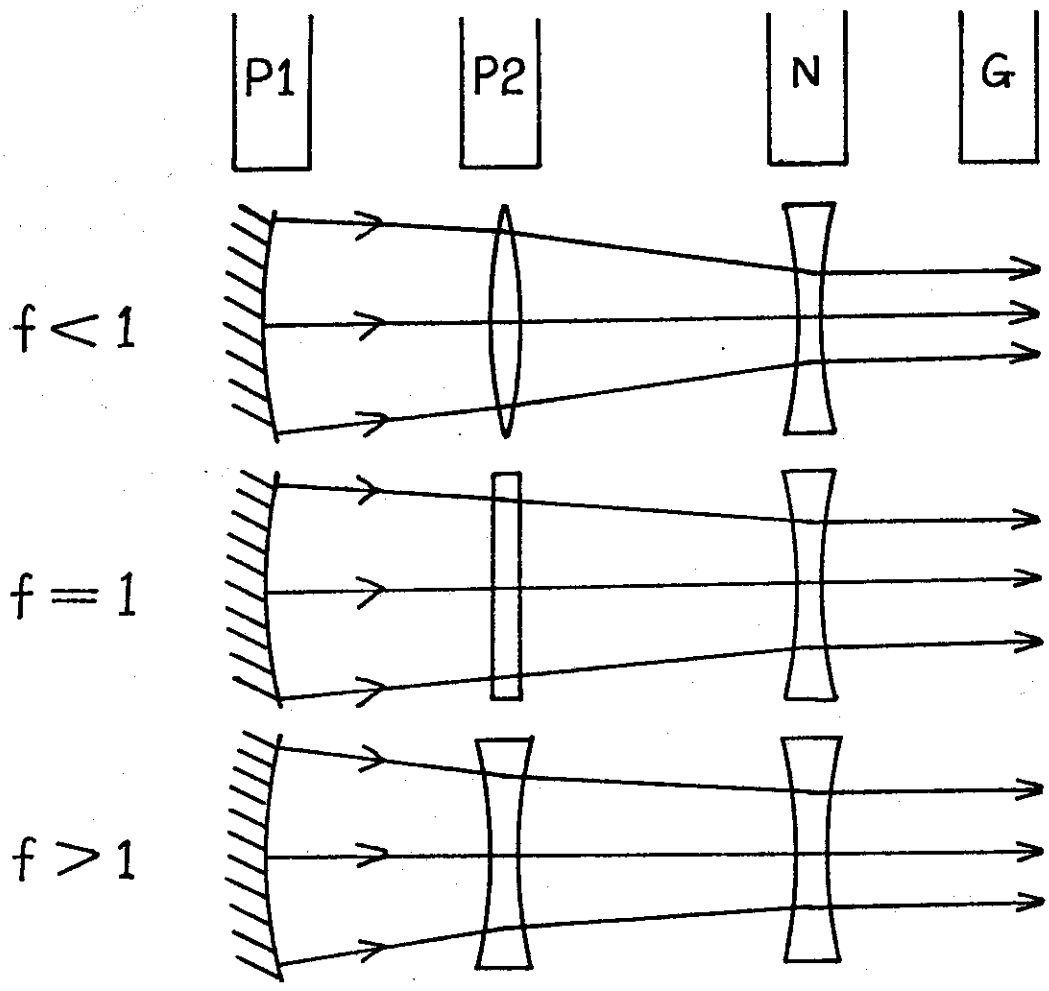

Fig. 2

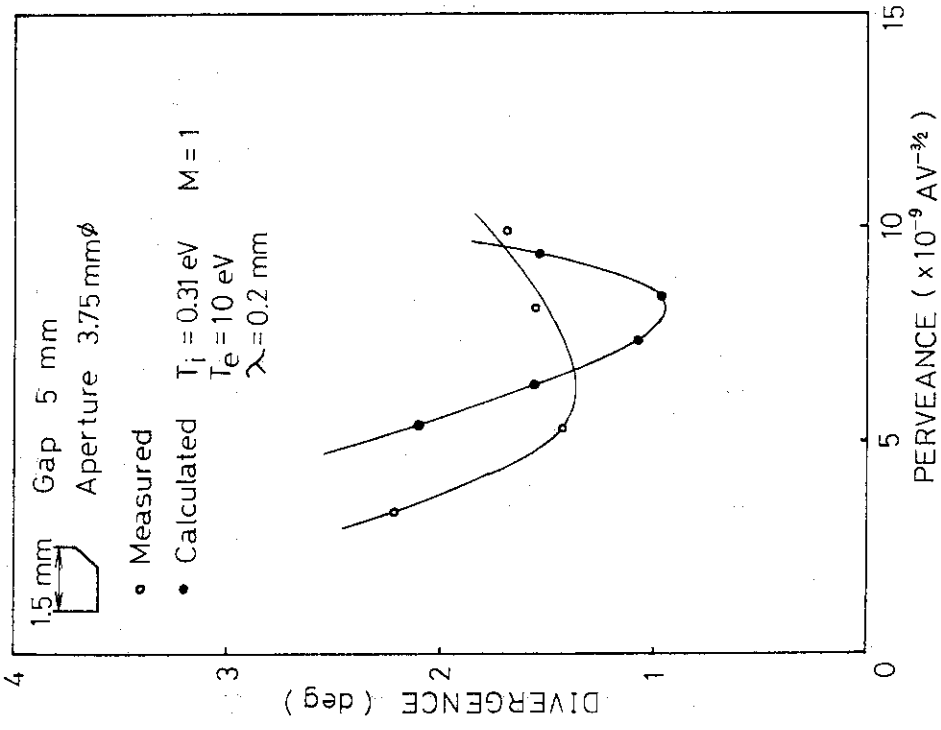
1.5 mm
Gap 5 mm
Aperture 3.75 mmϕ
∘ Measured
• Calculated
T_i = 0.31 eV
T_e = 10 eV
λ = 0.2 mm
M = 1
DIVERGENCE (deg)
PERVEANCE (×10⁻⁹ AV⁻³ᐟ²)

Fig. 3

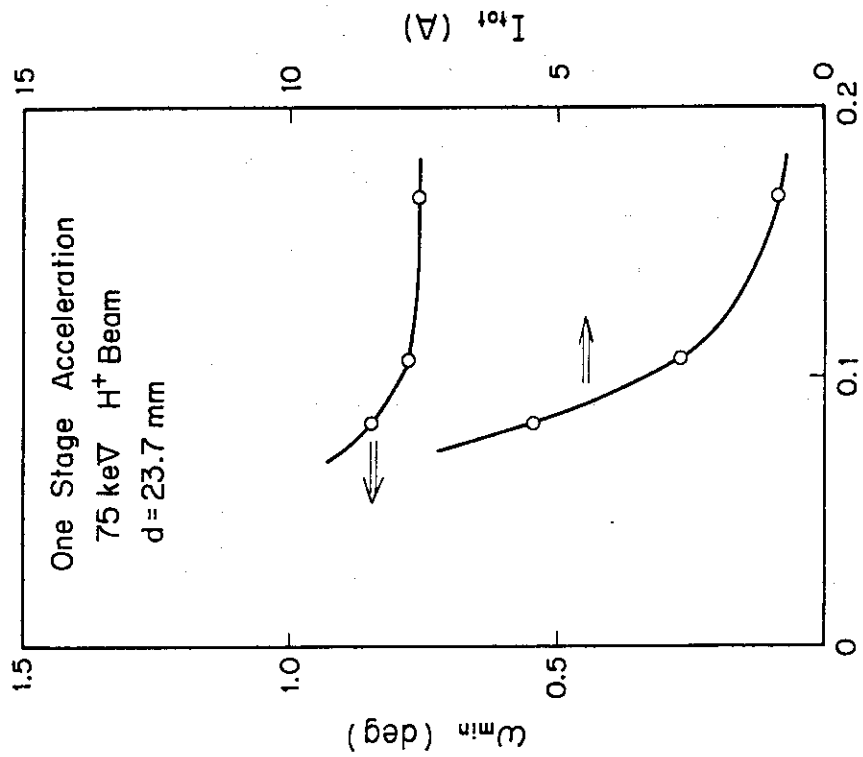
One Stage Acceleration
75 keV H⁺ Beam
d = 23.7 mm
ω_{min} (deg)
I_{tot} (A)
a

Fig. 4

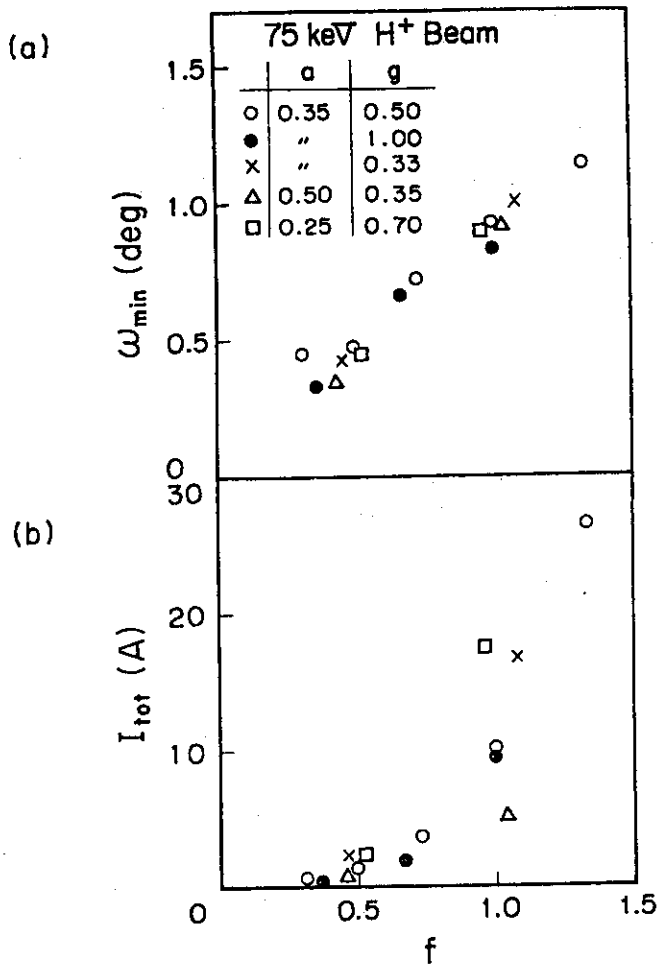
(a)
75 keV H+ Beam
a g
○ 0.35 0.50
● 〃 1.00
× 〃 0.33
△ 0.50 0.35
□ 0.25 0.70
ωmin (deg)
(b)
Itot (A)
f

Fig. 5

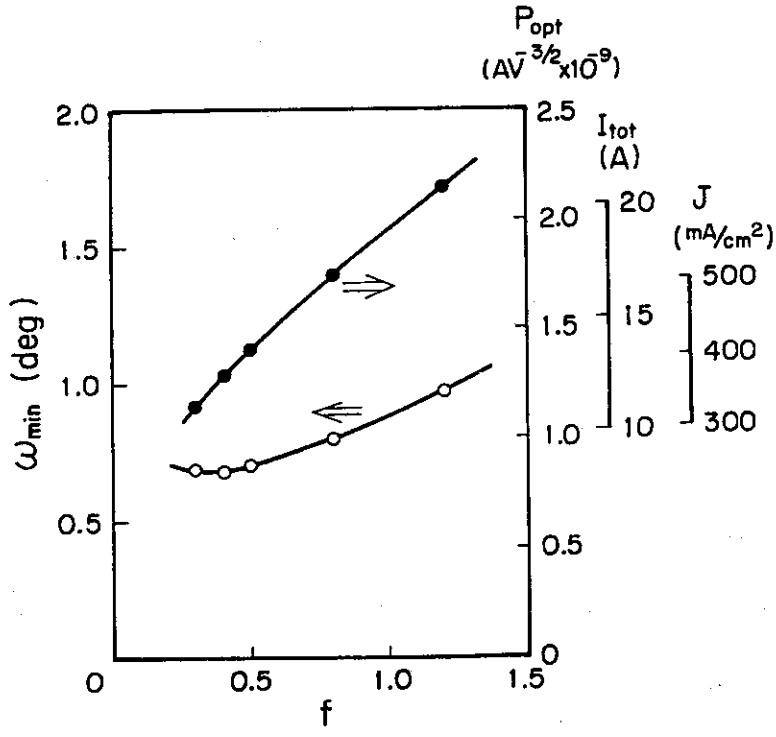
Popt
(AV-3/2x10-9)
Itot
(A)
J
(mA/cm2)
ωmin (deg)
f

Fig. 6

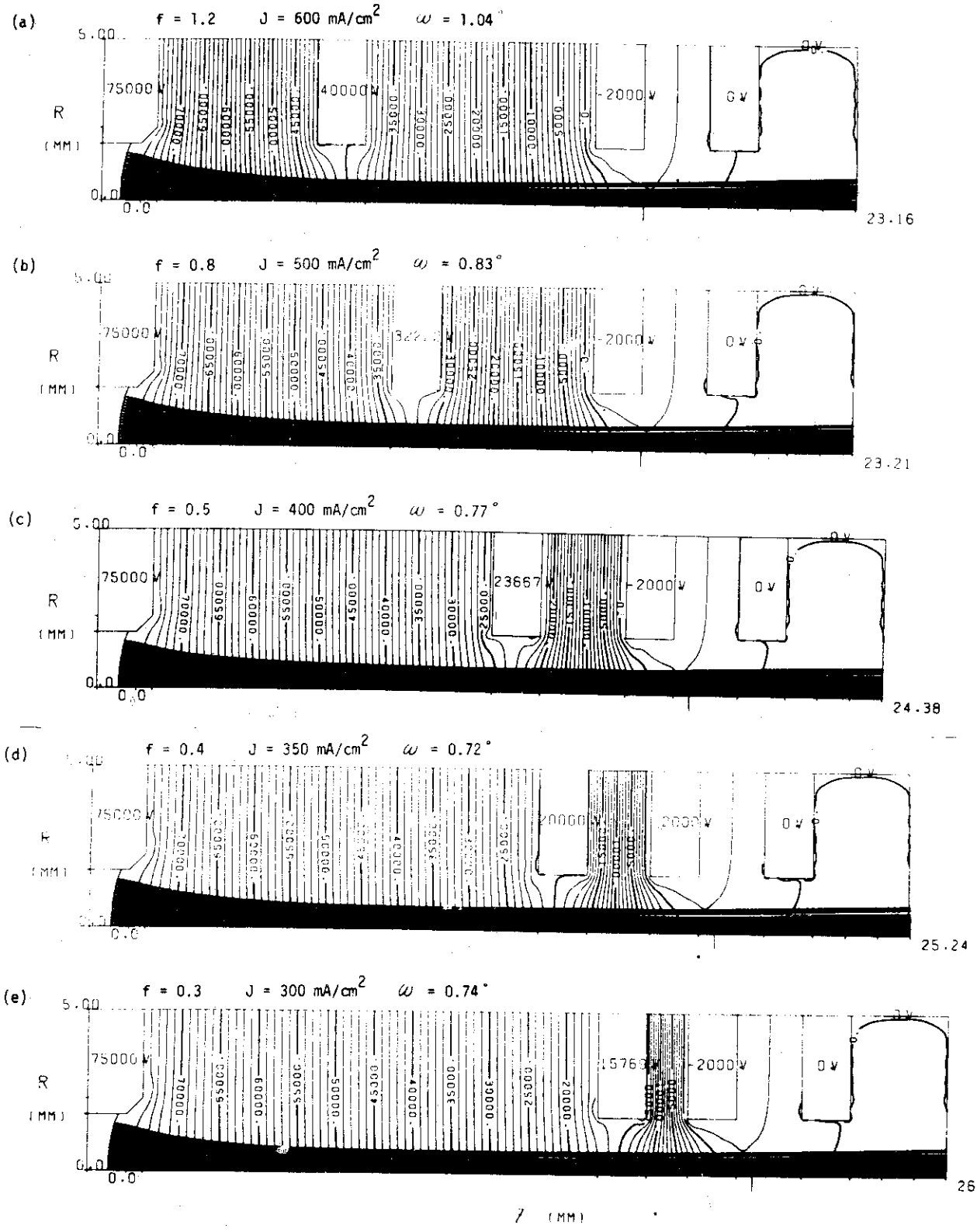
(a) f = 1.2 J = 600 mA/cm² ω = 1.04°
(b) f = 0.8 J = 500 mA/cm² ω = 0.83°
(c) f = 0.5 J = 400 mA/cm² ω = 0.77°
(d) f = 0.4 J = 350 mA/cm² ω = 0.72°
(e) f = 0.3 J = 300 mA/cm² ω = 0.74°
R (MM)
Z (MM)
75000 V
40000 V
23667 V
2000 V
0 V
23.16
23.21
24.38
25.24
26

Fig. 7

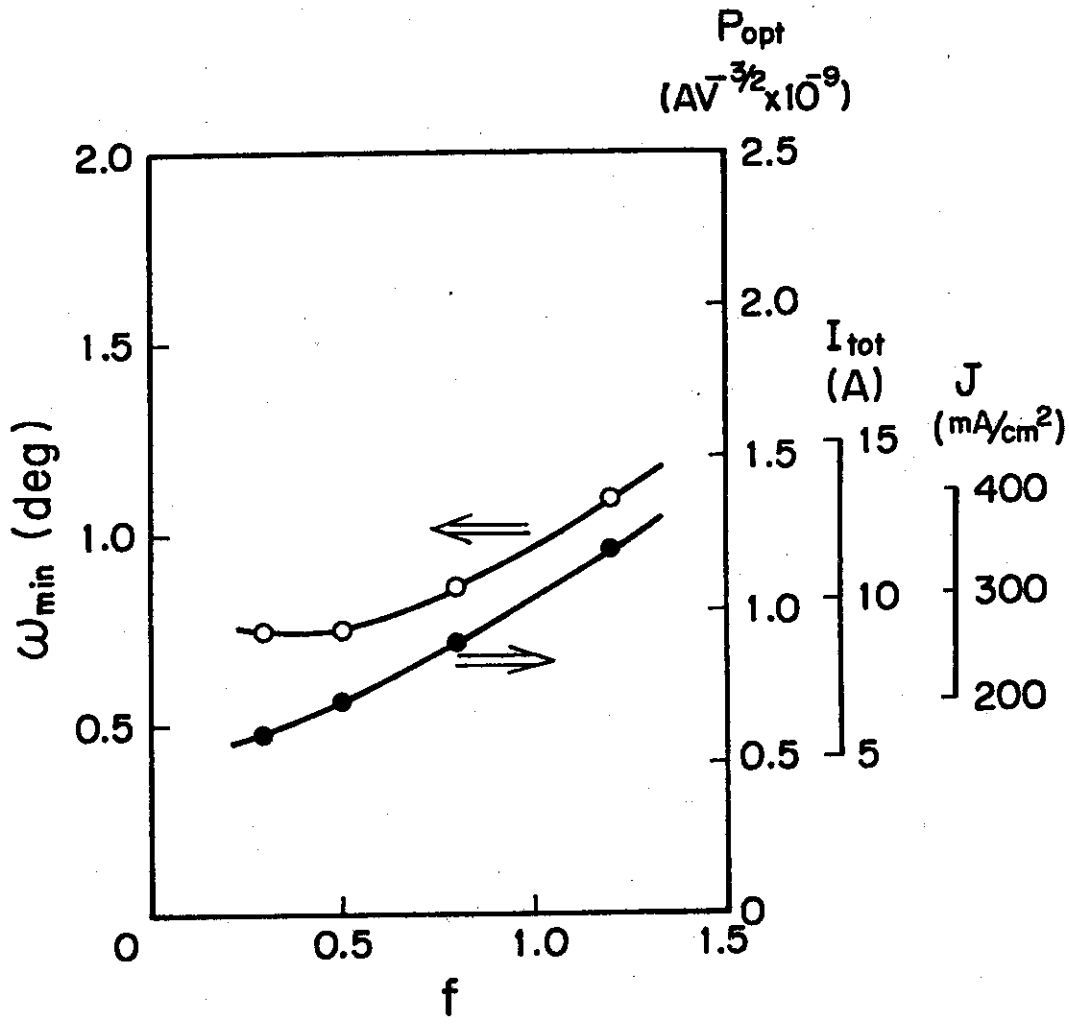
Popt
(AV^-3/2 x10^-9)
2.0
1.5
1.0
0.5
0
ωmin (deg)
2.5
2.0
1.5
1.0
0.5
0
Itot
(A)
15
10
5
J
(mA/cm²)
400
300
200
0.5
1.0
1.5
f

Fig. 8

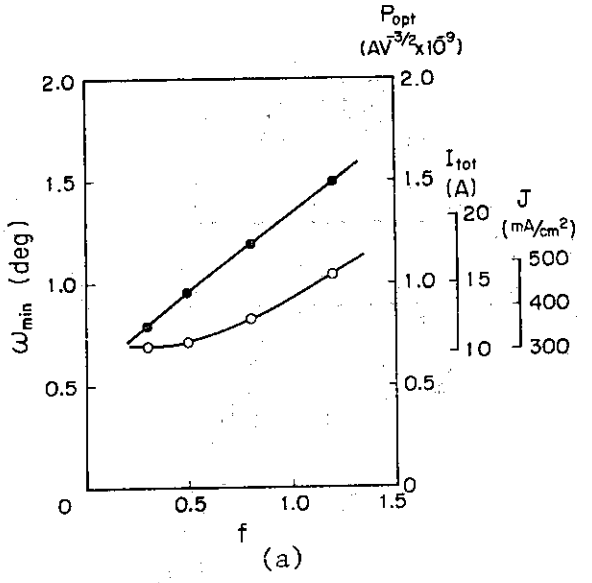
P_{opt}
$(AV^{-3/2}x10^{-9})$
ω_{min} (deg)
I_{tot} (A)
J
(mA/cm²)
f
(a)

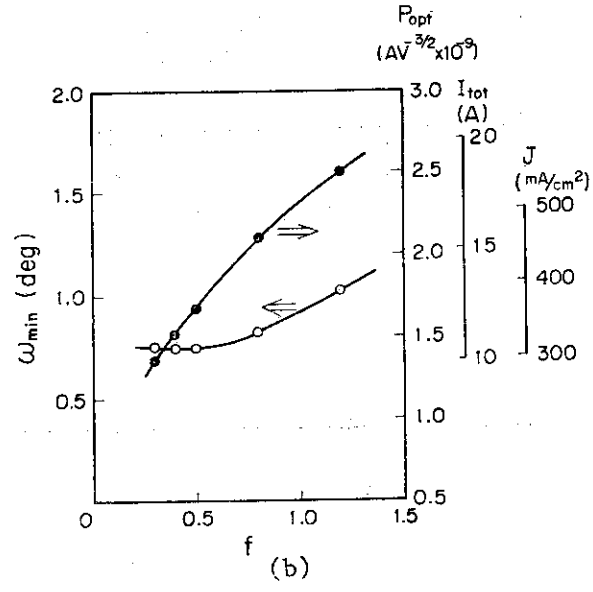
P_{opt}
$(AV^{-3/2}x10^{-9})$
ω_{min} (deg)
I_{tot} (A)
J
(mA/cm²)
f
(b)

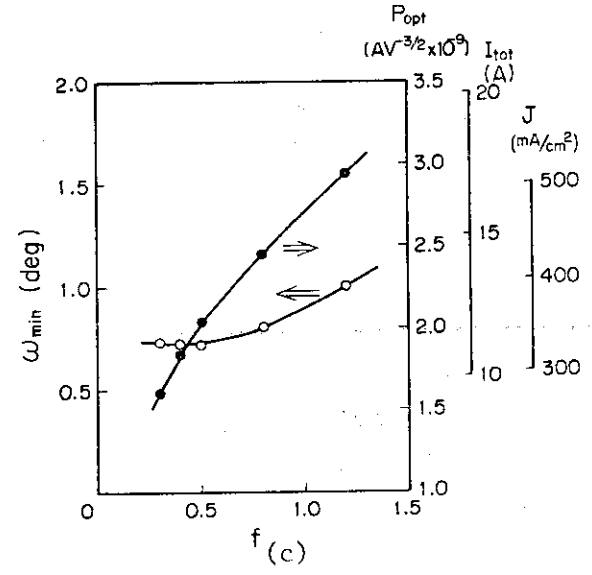
P_{opt}
$(AV^{-3/2}x10^{-9})$
ω_{min} (deg)
I_{tot} (A)
J
(mA/cm²)
f
(c)

Fig. 9

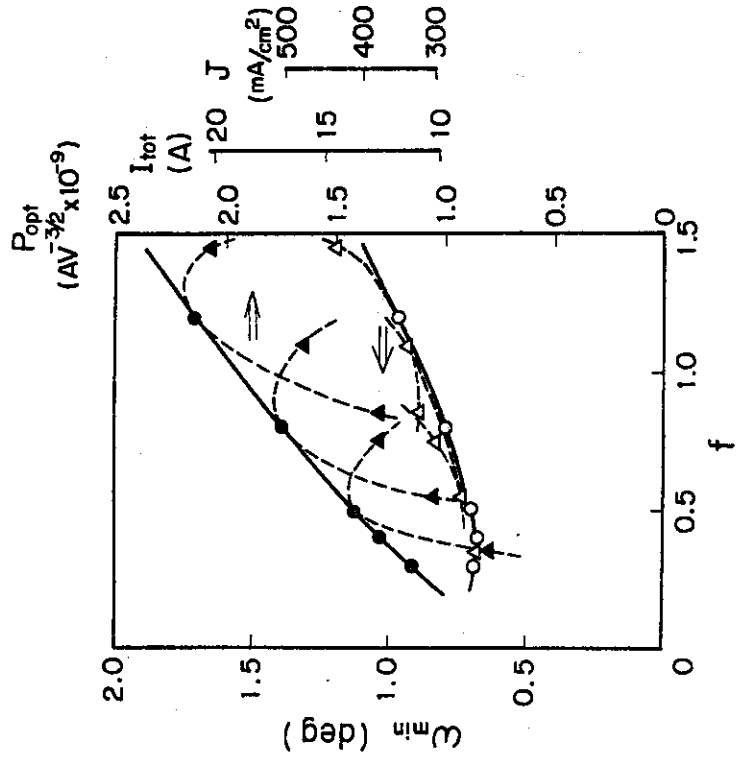
P_{opt} ($AV^{-3/2}x10^{-9}$)
I_{tot} (A)
J (mA/cm^2)
ω_{min} (deg)
f

Fig. 11

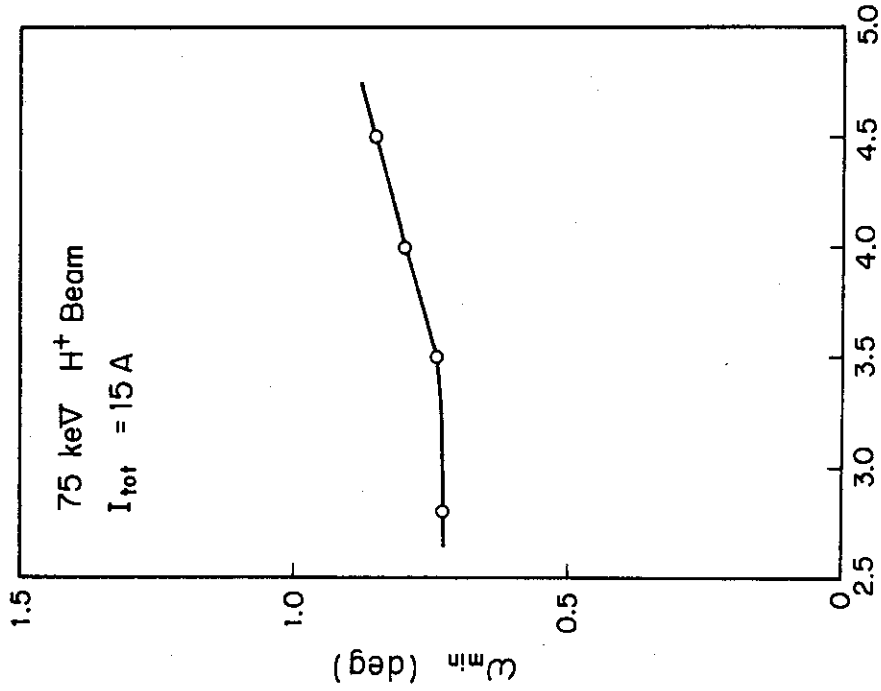
75 keV H^+ Beam
I_{tot} = 15 A
ω_{min} (deg)
$2r_1$ (mm)

Fig. 10

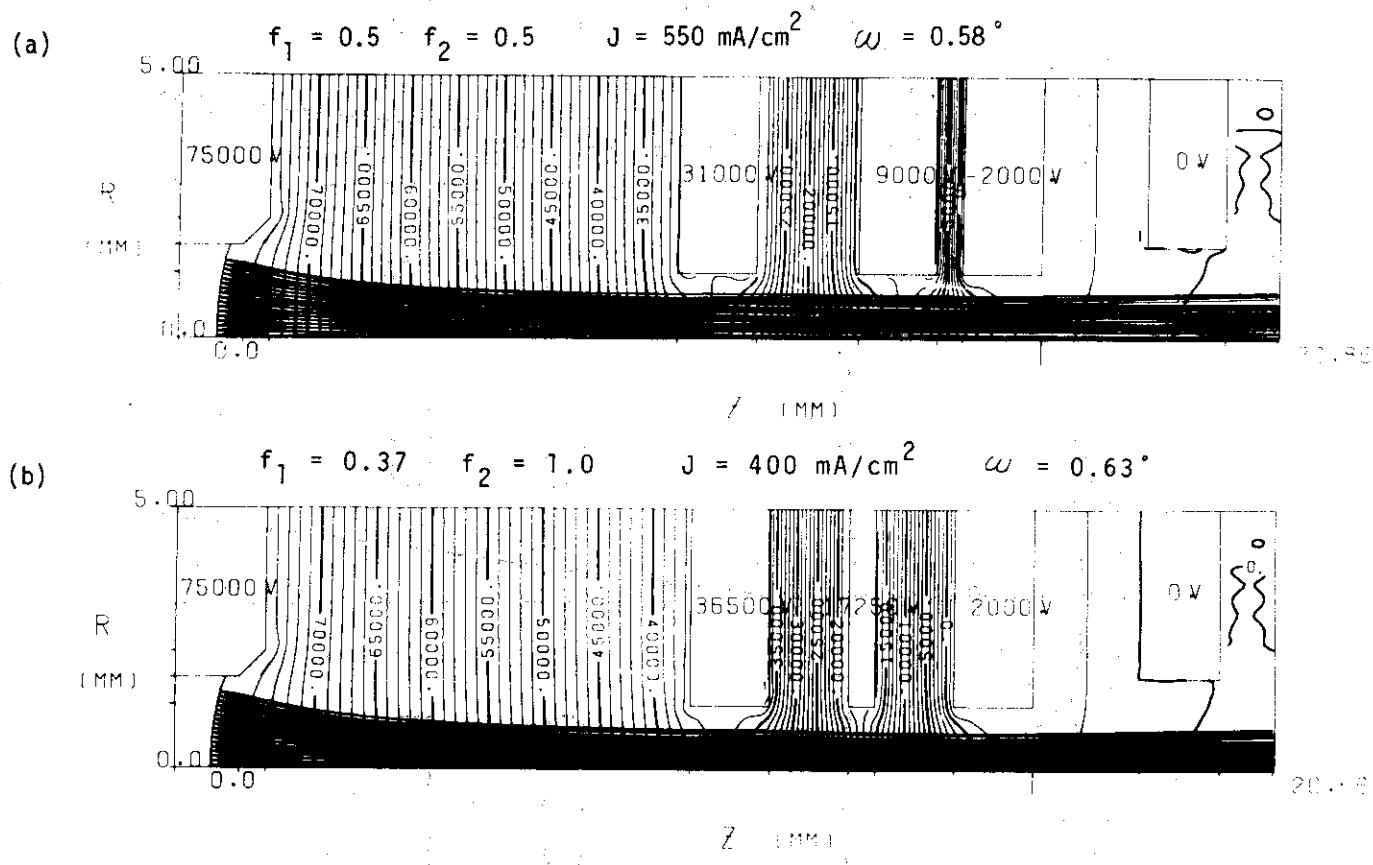
(a)
f_1 = 0.5 f_2 = 0.5 J = 550 mA/cm^2 ω = 0.58°
5.00
75000 V
70000
65000
60000
55000
50000
45000
40000
35000
31000 V
25000
20000
15000
9000 V
-2000 V
0 V
R (MM)
0.0
Z (MM)
(b)
f_1 = 0.37 f_2 = 1.0 J = 400 mA/cm^2 ω = 0.63°
5.00
75000 V
70000
65000
60000
55000
50000
45000
40000
36500 V
35000
30000
25000
20000
15000
10000
5000
0
2000 V
0 V
R (MM)
0.0
Z (MM)

Fig. 12

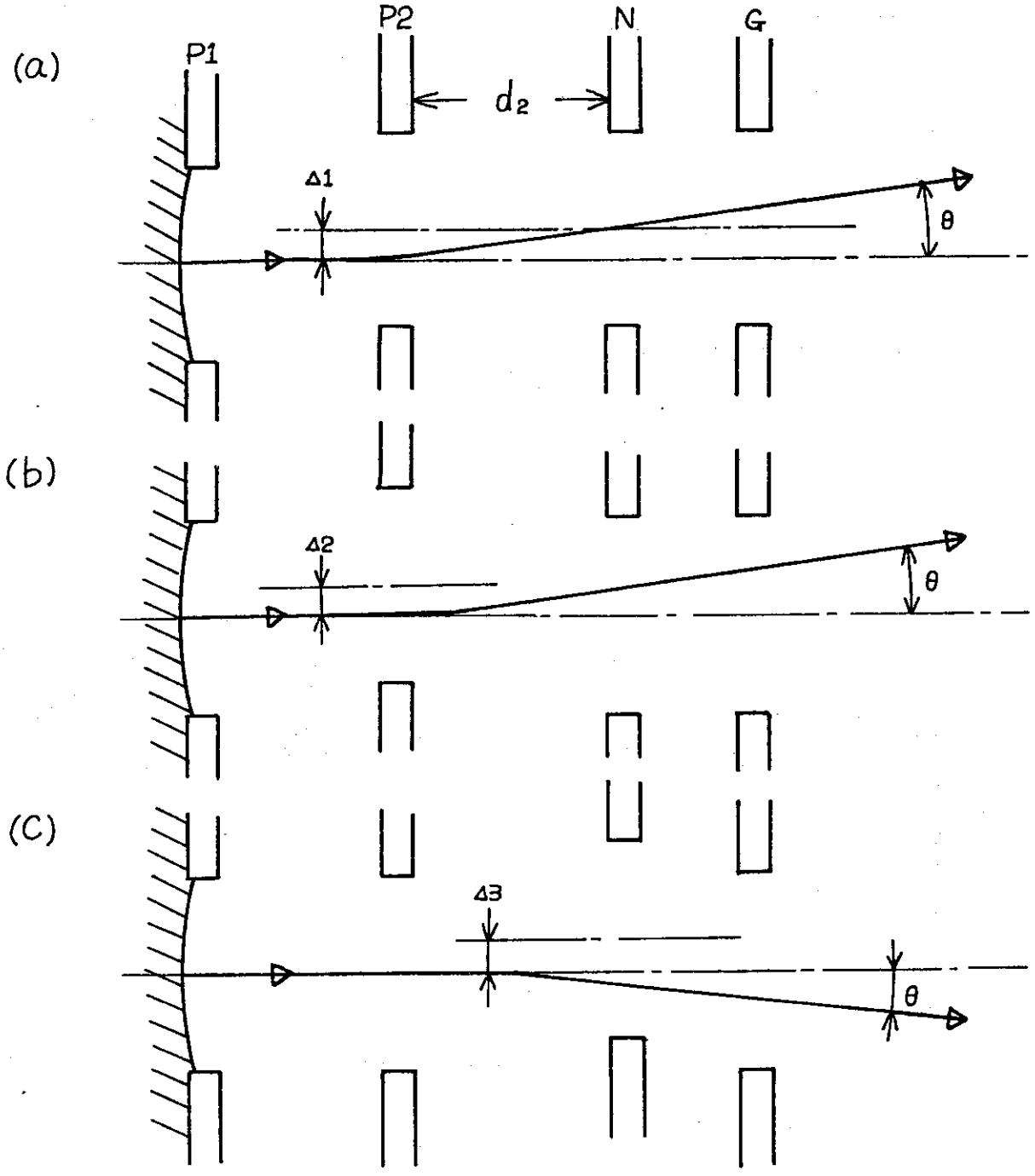

Fig. 13

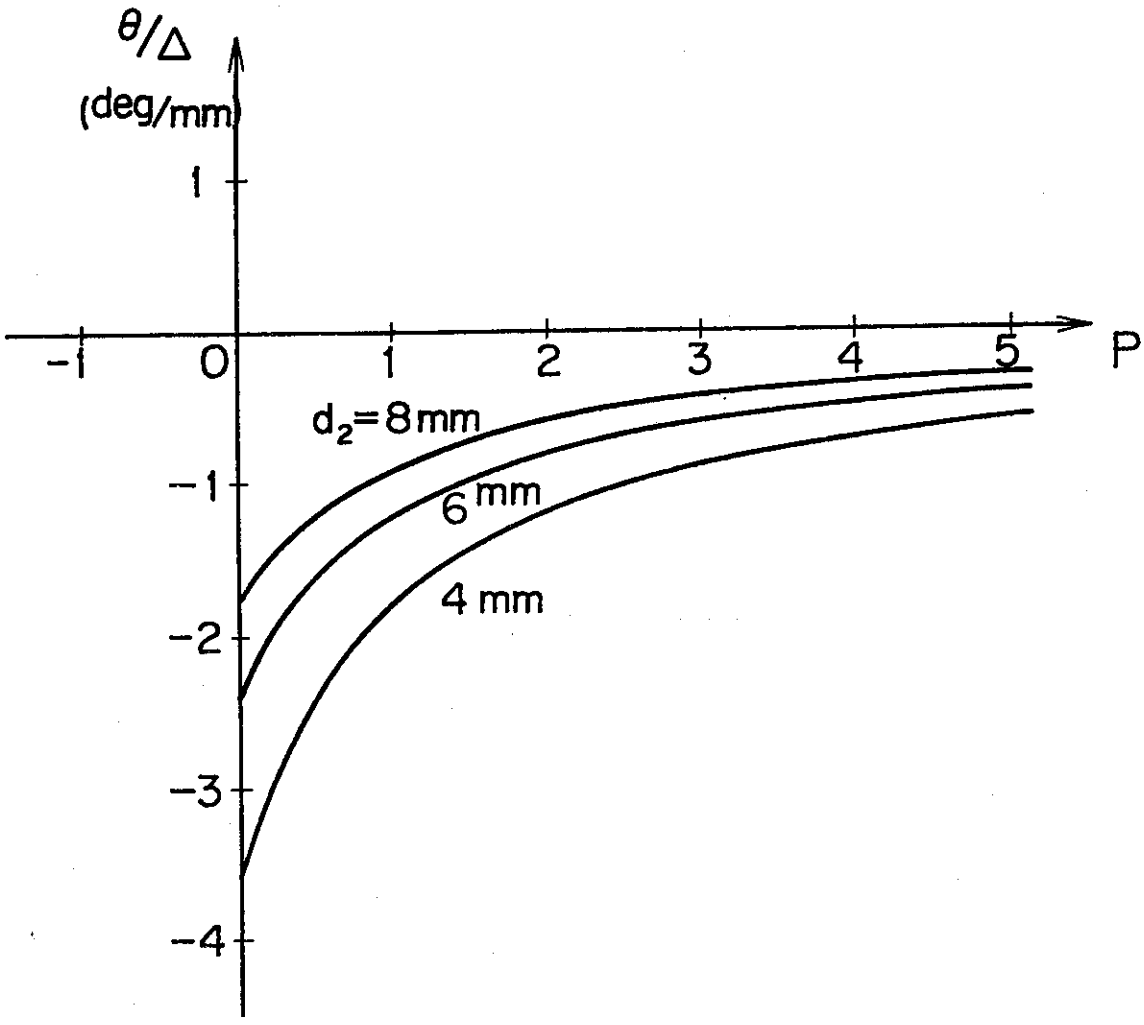

Fig. 14